

Seismic behavior of steel reinforced concrete cross-shaped column under combined torsion

Zongping Chen^{*1,2} and Xiang Liu^{1a}

¹ College of Civil Engineering and Architecture, Guangxi University, 100# east daxue road, Nanning, 530004, China

² Key Laboratory of Disaster Prevention and Structure Safety of Chinese Ministry of Education, Guangxi University, 100# east daxue road, Nanning, 530004, China

(Received July 21, 2017, Revised October 19, 2017, Accepted November 17, 2017)

Abstract. Experiments were performed to explore the hysteretic performance of steel reinforced concrete (SRC) cross-shaped columns. Nine specimens were designed and tested under the combined action of compression, flexure, shear and torsion. Torsion-bending ratio (i.e., 0, 0.14, 0.21) and steel forms (i.e., Solid - web steel, T - shaped steel, Channel steel) were considered in the test. Both failure processes and modes were obtained during the whole loading procedure. Based on experimental data, seismic indexes, such as bearing capacity, ductility and energy dissipation were investigated in detail. Experimental results suggest that depending on the torsion-bending ratio, failure modes of SRC cross-shaped columns are bending failure, flexure-torsion failure and torsion-shear failure. Shear - displacement hysteretic loops are fuller than torque - twist angle hysteretic curves. SRC cross-shaped columns exhibit good ductility and deformation capacity. In the range of test parameters, the existence of torque does not reduce the shear force but it reduces the displacement and bending energy dissipation capacity. What is more, the bending energy dissipation capacity increases with the rising of displacement level, while the torsion energy dissipation capacity decreases.

Keywords: steel reinforced concrete (SRC); cross-shaped column; compress-flexure-shear-torsion; combined action; seismic behavior

1. Introduction

Modern civilization has exerted people's aesthetic standards for architecture. The column extruding the wall affects the using functions of the architecture and causes people's visual uncomfortable. So special-shaped column, as L-shaped column, T-shaped column, cross-shaped column and so on, has began to replace traditional rectangle section column. Column limb of special-shaped column, as thick as filler wall, refrains from the exposure of prominence on the wall in interior space, which is conducive to the flexibility in the use of architectural space and comfortability of residence. Therefore, it is favored deeply by property owners and dwellers (Ramamurthy and Khan 1986, Zuo *et al.* 2012, Zhou *et al.* 2012).

In terms of materials, special-shaped column can be divided into several categories. Specifically, they are Steel (S) special-shaped column (Patton and Singh 2012), Reinforced Concrete (RC) special-shaped column (Li and Pham 2014), Concrete Filled Steel Tube (CFST) special-shaped column (Patton and Singh 2014), Steel Reinforced Concrete (SRC) special-shaped column (Liu *et al.* 2016) and so on. S special-shaped column is deficient in fireproofing and corrosion resistance (Sun *et al.* 2015). RC

special-shaped column doesn't have obvious advantages in bearing capacity, seismic resistance and building height, restricted to its own material property (Yang *et al.* 2010). CFST special-shaped column has 90 - degree internal corner, which weakens composite actions greatly between steel and concrete (Liang *et al.* 2008). Researches show that SRC special-shaped column has great advantages in seismic performance, such as high strength, stiffness and excellent ductility (Liu *et al.* 2016, Chen *et al.* 2016, Xiang *et al.* 2017, Fang *et al.* 2015). Apparently, compared with other three special-shaped columns, SRC special-shaped column shows strong functional and economical superiority.

Vast earthquake damages indicate that structures are damaged due to the additional twist of the column (Koliopulos and Chandler 1995). However, the structure design often overlooks the influence of torsion, which reduces the safety of structures (Arnold 1980, Duan and Chandler 2010). What is more, different from rectangular columns, the eccentricity between stiffness center and mass center of special-shaped columns often augments additional torque under the action of horizontal earthquake. Therefore, the failure mechanism of SRC special-shaped columns under compression, bending, shearing and torsion action should be given the appropriate attention.

However, little literature can be found about the seismic performance of SRC special-shaped columns under combined torsion except for some other kinds of members. Researches showed that torsion - bending ratio (T/M) have significance effects on seismic performance. Nie *et al.*

*Corresponding author, Ph.D., Professor,
E-mail: zpchen@gxu.edu.cn

^a Ph.D. Student

(2012, 2013) studied the seismic performance of concrete filled circular / rectangular steel tube columns under combined torsion. They found that with the increasing of T/M ratio, the bending capacity decreased, while the torsion capacity increased. Other researchers, such as Otsuka *et al.* (2005), Hsu *et al.* (Hsu and Wang 2000, Hsu *et al.* 2004), Tirasit and Kawashima (2007) also found the same interaction effect between torsion and flexure. Li and Belarbi (2012, 2013) did research with 3 circular RC bridge columns and 4 square RC bridge columns. They pointed out that the location and length of damage zone moved upward from the base of the column as the T/M ratio increased, with the failure mode and deformation characteristics changed.

Investigation showed that structure of the member can also affect its seismic performance. Belarbi *et al.* (2007) and Prakash *et al.* (2010) did a series of specimens under pure torsion, pure flexure and combined torsions. Their results showed a significant change in failure modes and deformation characteristics not only due to T/M ratio, but also the aspect ratio and spiral reinforcement ratio.

Wang *et al.* (2014) found that the decreasing of stirrup spacing can improve the torsion strength of columns, but it had little influence on the bending performances,

which is the same conclusion as Deng *et al.* (2017).

Anumolu *et al.* (2016) developed a three - dimensional model of HC-SCS column under combined torsion by finite element, what is more, they also developed a simplified equation to predict the torsion strength. Mullapudi (2013) put forward a three - dimensional model of RC members subjected to combined torsion. They used the model to assess the seismic performance, which also fits the experimental results well.

Cross-shaped column is one of the main forms of special-shaped columns. But previous literatures show that there have been few studies on the hysteretic behavior of SRC cross-shaped columns under combined loadings of compression, flexure, shear and torsion. Besides, the interaction between flexural and torsion of SRC cross-shaped columns is also limited. In order to expand the application of SRC cross-shaped columns, nine specimens with different T/M ratios and shaped - steel layouts were fabricated, and reversed cyclic tests subjected to compression, bending, shear, torsion were performed. The effects of combined torsion on failure modes, torque - twist angle and shear - displacement hysteretic curves, backbone curves, bearing capacity, ductility, energy dissipation and stiffness were discussed.

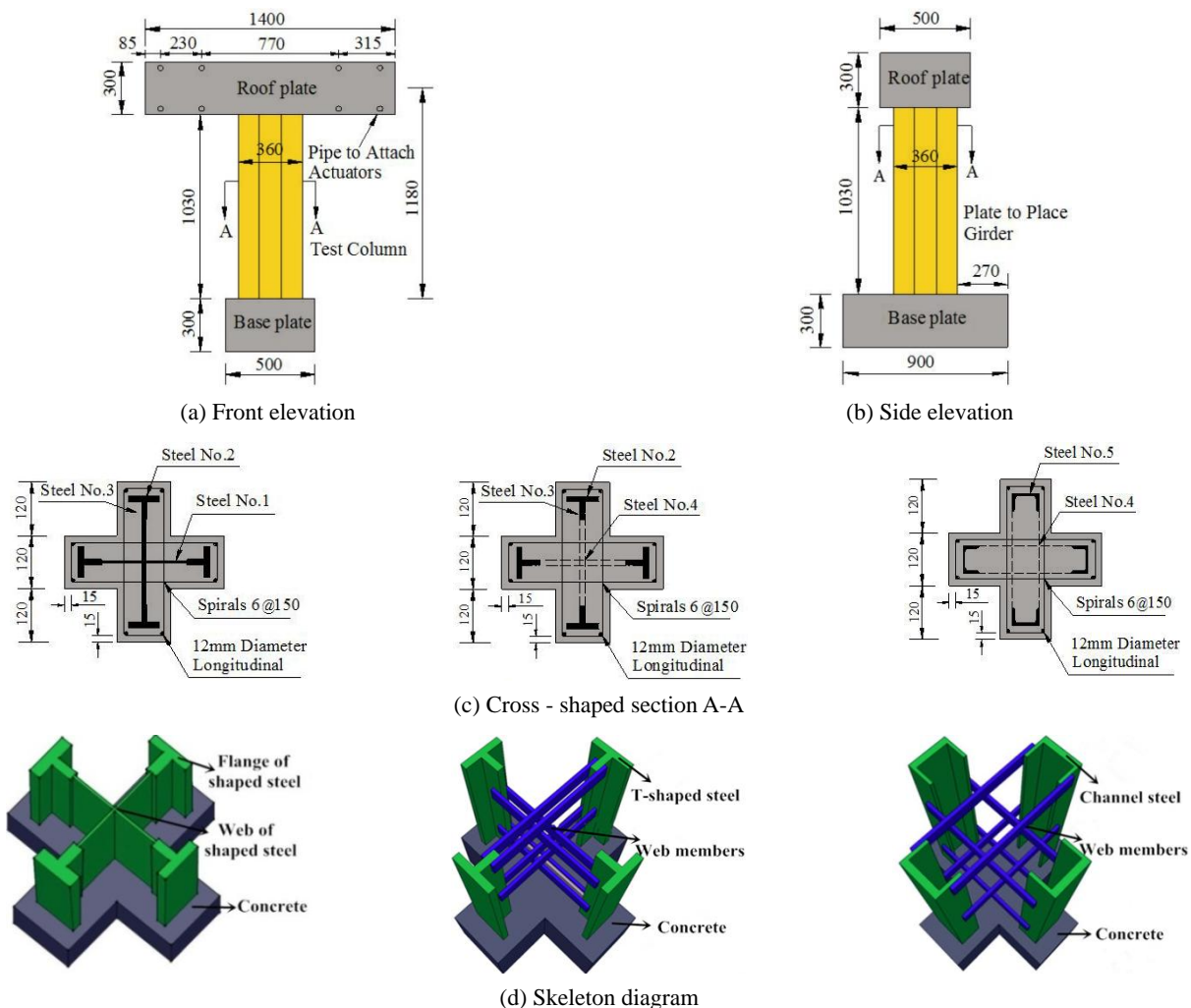


Fig. 1 Detailed design of specimens (Unit: mm)

Table 1 Parameters and load steps of specimen

No.	Steel forms	Steel content	T/M ratio	L - control F_1/F_2	D - control Δ_1/Δ_2	Axial compress ratio	Shear span ratio
SRC-1	solid-web	9.90	0.21	3	3	0.17	3.0
SRC-2	solid-web	9.90	0.14	2	2	0.17	3.0
SRC-3	solid-web	9.90	0.00	1	1	0.17	3.0
SRC-4	T-shaped	8.36	0.21	3	3	0.17	3.0
SRC-5	T-shaped	8.36	0.14	2	2	0.17	3.0
SRC-6	T-shaped	8.36	0.00	1	1	0.17	3.0
SRC-7	channel	6.74	0.21	3	3	0.17	3.0
SRC-8	channel	6.74	0.14	2	2	0.17	3.0
SRC-9	channel	6.74	0.00	1	1	0.17	3.0

Table 2 Steel material properties

Steel No.	Steel size/mm	f_y /MPa	f_u /MPa	$E_s \times 10^{-5}$ MPa
1	1230×184×5	306.54	430.08	1.85
2	1230×40×12	402.44	533.74	1.72
3	1230×70×12	311.75	450.76	1.83
4	200×25×8	402.02	539.66	1.91
5	channel steel	426.19	596.35	1.71
6	1230×12	498.42	667.08	2.02
7	1230×6	443.21	611.34	1.99

2. Experimental programs

2.1 Specimens details

Nine specimens were designed and fabricated to be representative of typical SRC cross-shaped columns as shown in Fig. 1. All specimens were the same geometry size. The total height was 1630 mm with an effective height of 1180 mm measured from the bottom of column to the centerline of loading points. Height and thickness of column limb were 360 mm and 120 mm, respectively. SRC roof plate size was 1400×500×300 mm, SRC base plate size was 900×500×300 mm. Shear span ratio was 3.0, clear concrete cover was 15 mm and constant axial compression ratio was 0.17. Eight 12 mm - diameter steel bars were used as longitudinal reinforcements and ten 6mm - diameter steel bars were used as stirrups. All specimens were tested under combined loading at T/M ratios of 0.00, 0.14 and 0.21. The specimen was subjected to pure bending when the T/M = 0. The shaped-steel layouts included solid-web steel, T-shaped steel and channel steel. The specimen parameters are presented in Table 1.

2.2 Material properties

All specimens were made of commercial concrete, and three 150 mm cubes were cast and cured with column specimens in the same outdoor conditions. The concrete strength was measured just before the pseudo - static tests, and the average value was $f_{cu,m} = 39.3$ MPa.

Table 2 gives the properties of structure steel and steel bars, with the f_y , f_u and E_s represent the yield strength,

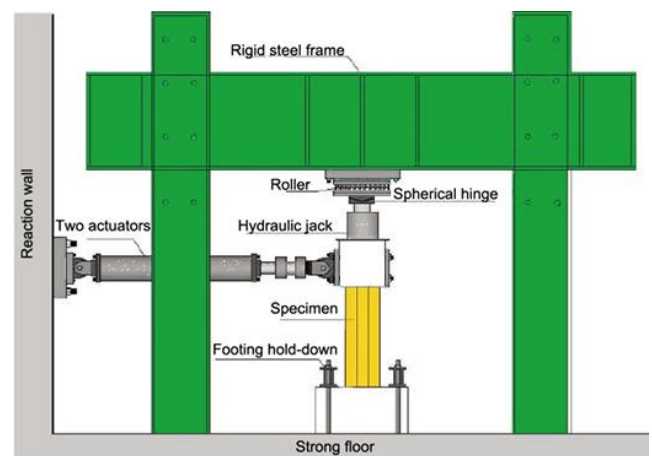


Fig. 2 Test setup

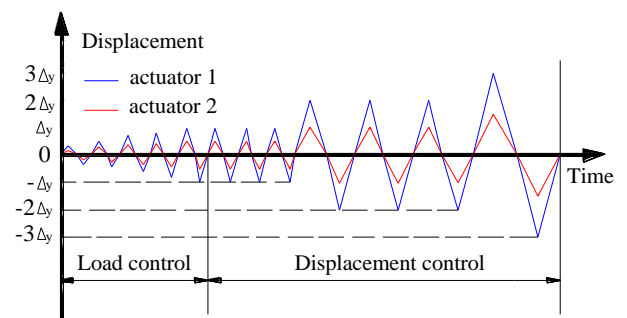


Fig. 3 Loading process

ultimate tensile strength and elastic modulus, respectively. The steel coupons used in the material characteristic test were cut from the structure steel and steel bars.

All the material characteristic tests were conducted according to the Chinese codes “Metal materials tensile test at room temperature” (2010) and “Ordinary concrete mechanics performance test method standard” (2002).

2.3 Test setup and procedure

Test setup offering combined compressing, bending, shear and torsion is shown in Fig. 2. The base plate was fixed by four steel reaction screws and two steel girders. A constant vertical - axis compression was applied by a hydraulic jack. Rollers were set between the hydraulic jack and reaction frame in order to do not restrain lateral displacement. Spherical hinge was set between the hydraulic jack and the roof plate in order to do not restrain twist angle. Two electro-hydraulic servo actuators were used to offer the horizontal loading at the roof plate. Then, the combined bending and torsion was generated by controlling forces (F_1 , F_2) and displacements (Δ_1 , Δ_2) with each actuator as the designed loading process. Different T/M ratios were imposed by applying the two actuators with different ratios of force and displacement. Horizontal displacements of the specimen were measured by displacement sensors installed in electro-hydraulic servo actuators. The loading steps of each actuator are given Table 1.

The loading equipment is checked by applying thirty percent of the axial load and monitoring the corresponding readings of all instruments. If all are in order, the targeted constant axial load will be applied and maintained during the test, whereas the lateral forces are cycled. The loading process includes load - controlled phase and displacement - controlled phase, which is illustrated in Fig. 3. During the load - controlled stage, every load amplitude is conducted in single cycle. When the specimen first yielded, the loading process entered into displacement - controlled phase. The horizontal displacement corresponding to the first yield point is named yield displacement Δ_y , which is taken as the cyclic displacement times for loading amplitude ($n\Delta_y$, n is an integer). In the displacement - controlled phase, each displacement amplitude is conducted in three cycles to measurement the indication of strength and stiffness degradation characteristics. The test finishes until the lateral loads resistance deteriorate to 85% of the maximum measured lateral loads.

3. Failure modes

With the increase of T/M ratio, the failure pattern translates from bending failure (T/M = 0) to bending-torsion failure (T/M = 0.14) and torsion - shear failure (T/M = 0.21). The cracks and failure patterns are shown in Fig. 4. The red cracks represent pull and blue cracks represent push.

3.1 Bending failure

Specimens with T/M = 0 (SRC-3, SRC-6, SRC-9) are

bending failure. Take the damage process of SRC-3 as an example: SRC-3 exhibited first horizontal flexural crack on the column limb parallel to the loading direction when loaded into 55 kN. As the load continued to increase, the original crack extended and widened. At the same time, new horizontal cracks appeared. Under the action of repeated loading, horizontal cracks developed alternately on the column limbs parallel to the loading direction, especially in the middle and lower part. However, there were little cracks on the column limbs vertical to the loading direction due to they were near the neutral axis. At the end of the test, many longitudinal cracks (about 150 mm height) appeared on the base of the column limb parallel to the loading direction, followed by concrete crush.

3.2 Bending - torsion failure

Specimens with T/M = 0.14 (SRC-2, SRC-5, SRC-8) are bending - torsion failure. Take the damage process of SRC-2 as an example: the early progress of SRC-2 was similar to SRC-3 with the horizontal cracks arose firstly. As the load increased, crack morphology showed new characteristics. The crack angles of SRC-2 increased from 0° to 45°, and developed crosswise and helically on column limbs both parallel and vertical to the loading direction. At the end of the test, longitudinal cracks (about 200 mm height) appeared on the base of the column limb parallel to the loading direction, followed by concrete crush.

3.3 Torsion - shear failure

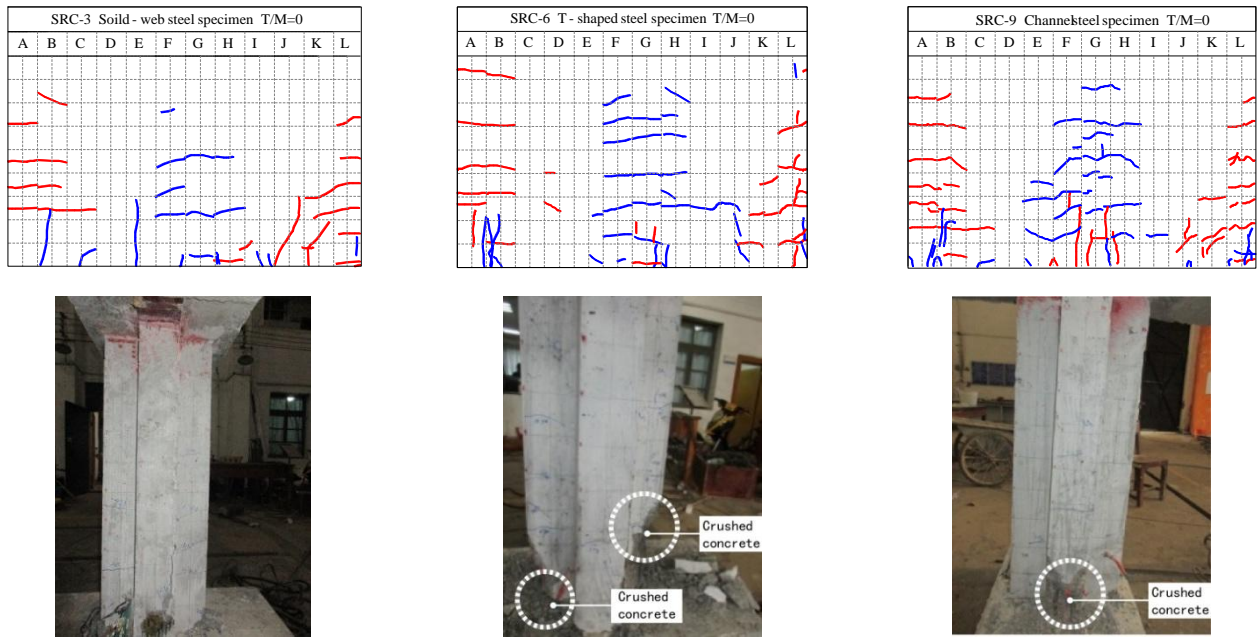
Specimens with T/M = 0.21 (SRC-1, SRC-4, SRC-7) are torsion - shear failure. Take the damage process of SRC-1 as an example: when loaded into 42 kN, the first diagonal crack appeared on the column limb parallel to the loading direction in the middle part. The cracks gradually intersected in a cross with their angle increased from 45° to 65°. The width of those cracks expanded, which prompted to form several big diagonal cracks. And then some longitudinal cracks appeared on each column limbs with 600 mm height, which caused the cover concrete peeling.

It can be seen from Fig. 4 that specimens with same T/M ratio had the same failure mode even the shaped - steel layout was different, which indicated the failure modes was mainly affected by the T/M ratio. The distribution range, quality and angles of cracks were likely to expand as T/M ratio increased. This indicated that the specimens had more flexure characteristics when the T/M ratio was small, and more torsion failure characteristics when the T/M ratio was large. When the T/M = 0.00, 0.14 and 0.21, the angles were mainly 0°, 30~45° and 45~65°, respectively.

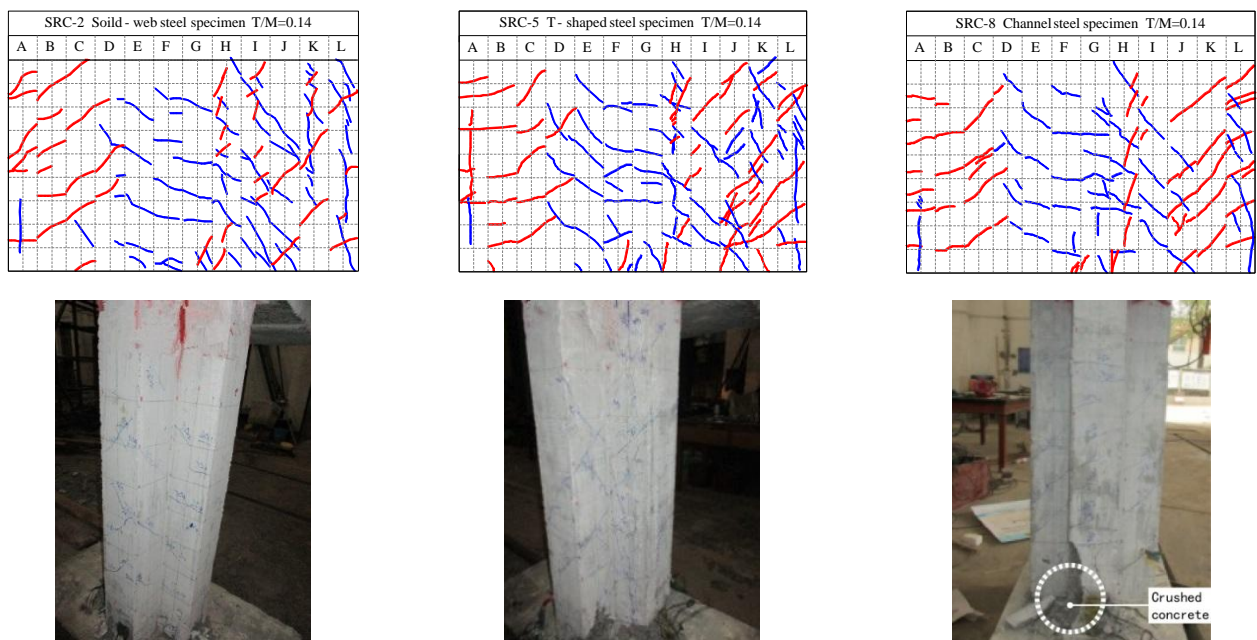
4. Test results analysis

4.1 Hysteretic behavior

Figs. 5 and 6 show torque-twist angle and shear-displacement hysteretic curves, respectively. T represents torque, θ represents twist angle, P represents shear and Δ represents displacement.



(a) Specimens of $T/M = 0$



(b) Specimens of $T/M = 0.14$



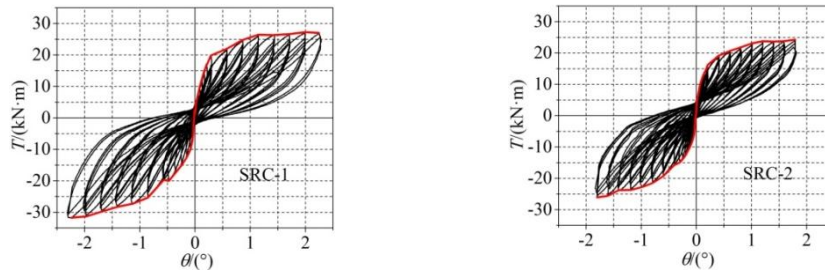
(c) Specimens of $T/M = 0.21$

Fig. 4 The failure pattern and cracks distribution

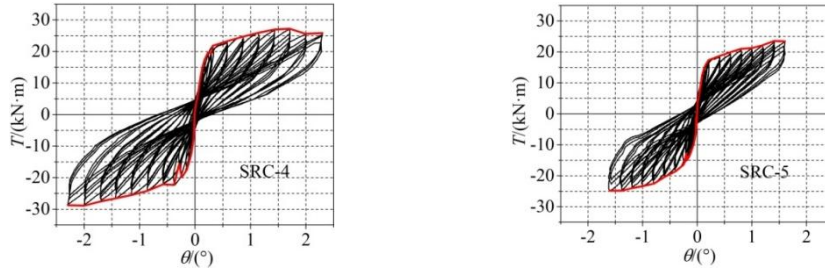
* Note: the blue line is positive direction (push), and the red line is reverse direction (pull) in Fig. 4

Hysteretic loops are nearly symmetry, shows pinched S - shaped basically, while the shear-displacement hysteretic loops are plumper. The specimens damaged mainly because

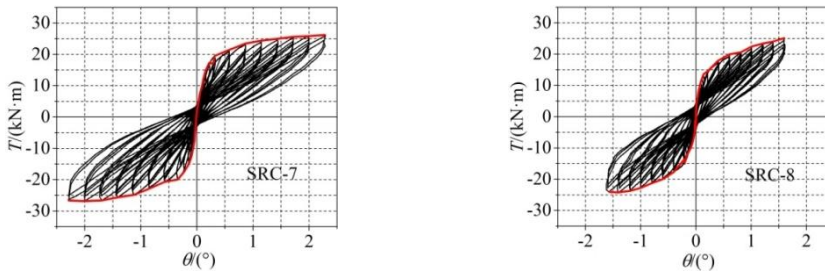
of the shear force, which decreases to 85% of its maximum value. However, the torque nearly keeps constant, showing good torsion bearing capacity. The torque of SRC crossed –



(a) Solid - web steel specimens

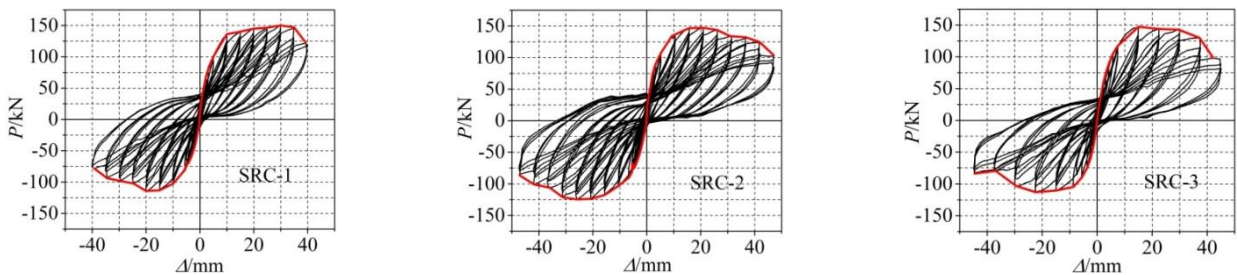


(b) T - shaped steel specimens

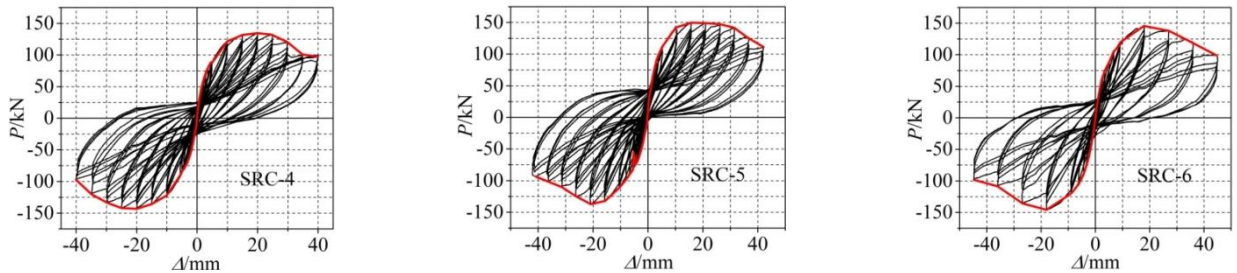


(c) Channel steel specimens

Fig. 5 Torque - twist angle hysteretic curves (T/M ratio decreases from left to right)

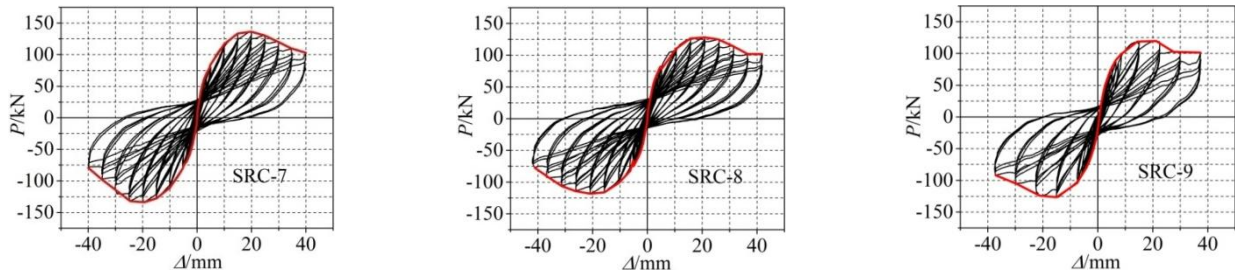


(a) Solid - web steel specimens



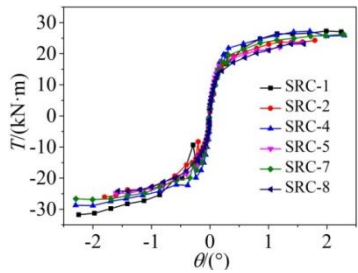
(b) T - shaped steel specimens

Fig. 6 Shear - displacement hysteretic loops (T/M ratios decrease from left to right)

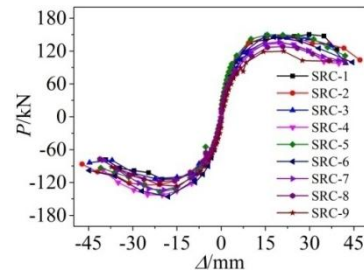


(c) Channel steel specimens

Fig. 6 Continued



(a) Torque - twist angle backbone curves



(b) Shear - displacement backbone curves

Fig. 7 Backbone curves

shaped column is mainly depended on the strength of steel web plate, lacing bars and stirrups, while the shear force is mainly controlled by the strength of steel flange and longitudinal reinforcements. When damage occurs under interaction stress, the steel web plate, lacing bars, stirrups and confined concrete can still take part in the torsion resistance as a whole.

During load - controlled phase, the hysteretic curves extends linearly with no residual deformation surrounding, which implies that the specimens are in elastic state. During displacement - controlled phase, the hysteretic curves tilt gradually to twist angle and displacement axis, indicating that stiffness deterioration and damage accumulation occurs in the specimens. The hysteretic curve area in the displacement - controlled phase is much larger than that in the load - controlled phase, showing a better energy dissipation capacity. After maximum load, when the load resistance descends to zero, simultaneously, the lateral displacement remains a positive value, which reflects the residual deformation and hysteresis phenomenon appeared. In addition, as the number of cycles increase, the residual deformation and hysteresis phenomenon become obviously, likewise, the area surrounded by hysteretic curves becomes smaller.

4.2 Backbone curves

Backbone curve envelopes are used to determine stiffness, ductility, and load carrying capacity. Torque - twist angle and shear - displacement backbone curves are shown in Fig. 7. Characteristic loads and displacements, corresponding to crack point, yield point, peak point and ultimate point from the backbone curves are presented in Table 3. The yield points are calculated according to energy equivalence method, the peak points refer to the points of

maximum loads, and ultimate points are equal to points of 0.85 maximum loads at the descending segment of backbone curves.

All the torque - twist angle and shear - displacement backbone curves contain linear elasticity segment, elastic - plastic segment and ultimate segment. Curves of initial stage were similar and their slopes are close, which reflect the influence of T/M ratios and shaped - steel layouts on the initial stiffness is not evident.

From Fig. 7(a) it can be seen that after linear elasticity segment, the torque increases slowly, while the twist angle increases considerable. The advantages on torsion ductility of the steel get evident. Table 3 shows that the increasing of T/M ratio from 0.14 to 0.21 leads to a respective increase in ultimate torque and twist angles. The comparison between SRC-1 (T/M = 0.21) and SRC-2 (T/M = 0.14) shows that with same steel layout, the ultimate torque of SRC-1 is larger than SRC-2 by 17%, and the twist angles is larger by 18%. Similarly, shaped - steel layout also has greatly effects on the ultimate torque and twist angles. With the same T/M ratio, ultimate torque of Solid - web specimens are the largest, followed by T - shape steel specimens and then the Channel steel specimens. Take the specimens of T/M = 0.14 for example, compared with SRC-8 (Channel steel specimen), the ultimate torque of SRC-5 (T - shaped steel specimen) extends by 6%, and that of SRC-2 (Solid - web specimen) extends by 12%. Specimens with solid - web steel have the largest ultimate twist angle, with the SRC-2 larger than SRC-5 by 29%, and larger than SRC-8 by 19%.

From Fig. 7(b) it can be seen that all shear backbone curves have gently descending stages, representing suitable ductility, especially for specimens with lower T/M ratios. When T/M ratio increases from 0.14 to 0.21, the ultimate displacement decreases, but the variation tendency of shear force is ambiguous, indicating that the influence of T/M

Table 3 Mechanical characteristics of loads and displacements

No.	Loading direction	Crack point				Yield point				Peak point			Ultimate point		
		T_{cr}	θ_{cr}	P_{cr}	Δ_{cr}	T_y	θ_y	P_y	Δ_y	P_m	Δ_m	T_u	θ_u	P_u	Δ_u
SRC-1	Push	12.7	0.13	67	1.3	22.5	0.63	132	9.4	150	29.9	27.3	1.99	128	38.4
	Pull	11.8	0.13	47	2.2	26.8	1.07	96	8.8	114	20.0	31.8	2.24	97	30.8
	Average	12.2	0.13	50	1.8	24.7	0.85	114	9.1	132	24.9	29.5	2.12	113	34.6
SRC-2	Push	10.5	0.07	63	1.6	20.0	0.52	121	7.3	147	20.9	24.3	1.80	125	41.7
	Pull	6.8	0.05	41	1.9	21.8	0.84	104	10.7	125	25.9	26.1	1.80	106	36.3
	Average	8.6	0.06	52	1.7	20.9	0.68	113	9.0	136	23.4	25.2	1.80	115	39.0
SRC-3	Push	—	—	76	3.0	—	—	123	8.8	148	15.0	—	—	125	37.9
	Pull	—	—	55	2.2	—	—	86	7.5	113	22.4	—	—	96	31.8
	Average	—	—	66	2.6	—	—	104	8.2	130	18.7	—	—	111	34.8
SRC-4	Push	16.0	0.15	64	2.3	22.9	0.51	111	8.4	135	19.9	27.2	1.71	114	31.4
	Pull	16.0	0.13	64	2.8	23.2	0.73	122	10.2	143	20.0	28.9	2.00	122	34.3
	Average	16.0	0.14	64	2.5	23.1	0.62	117	9.3	139	20.0	28.0	1.85	118	32.9
SRC-5	Push	14.2	0.11	86	2.7	19.3	0.50	123	7.0	150	15.7	23.6	1.41	127	36.0
	Pull	10.0	0.07	60	3.1	20.0	0.56	115	11.4	137	20.8	24.9	1.38	117	29.0
	Average	12.1	0.09	73	2.9	19.6	0.53	119	9.2	143	18.2	24.2	1.39	122	32.5
SRC-6	Push	—	—	68	2.8	—	—	122	10.0	146	17.9	—	—	124	33.6
	Pull	—	—	64	2.5	—	—	119	10.0	146	18.0	—	—	124	30.8
	Average	—	—	66	2.7	—	—	121	10.0	146	17.9	—	—	124	32.2
SRC-7	Push	14.7	0.15	59	2.4	21.8	0.63	114	9.5	137	19.8	26.2	2.29	116	31.7
	Pull	11.0	0.08	44	1.7	21.5	0.67	112	10.5	134	19.4	26.9	2.01	114	30.2
	Average	12.8	0.12	52	2.0	21.7	0.65	113	10.0	135	19.6	26.5	2.15	115	30.9
SRC-8	Push	12.0	0.10	72	3.7	18.5	0.57	105	9.5	128	20.9	23.2	1.61	109	33.6
	Pull	9.5	0.09	58	3.0	19.9	0.59	98	9.8	118	20.9	24.2	1.40	101	33.3
	Average	10.7	0.09	65	3.3	19.2	0.58	102	9.7	123	20.9	23.7	1.51	105	33.5
SRC-9	Push	—	—	67	3.9	—	—	102	9.4	120	21.2	—	—	102	35.0
	Pull	—	—	46	1.3	—	—	105	7.9	127	15.0	—	—	108	28.6
	Average	—	—	55	2.6	—	—	104	8.7	123	18.1	—	—	105	31.8

Table 4 Mechanical characteristics of deformation

No.	Direction	$\gamma_{cr}/\%$	$\gamma_u/\%$	$\mu_{\Delta} = \Delta_u/\Delta_y$	No.	Direction	$\gamma_{cr}/\%$	$\gamma_u/\%$	$\mu_{\Delta} = \Delta_u/\Delta_y$
SRC-1	Push	0.11	3.2	4.09	SRC-2	Push	0.13	3.6	5.71
	Pull	0.19	2.6	3.50		Pull	0.16	3.0	3.39
	Average	0.15	2.9	3.79		Average	0.15	3.3	4.55
SRC-3	Push	0.25	3.2	4.31	SRC-4	Push	0.19	2.6	3.74
	Pull	0.19	2.7	4.24		Pull	0.24	2.9	3.36
	Average	0.22	2.9	4.27		Average	0.21	2.8	3.55
SRC-5	Push	0.23	3.0	5.14	SRC-6	Push	0.24	2.9	3.36
	Pull	0.26	2.4	2.54		Pull	0.23	2.6	3.08
	Average	0.24	2.8	3.84		Average	0.23	2.7	3.22
SRC-7	Push	0.20	2.7	3.34	SRC-8	Push	0.31	2.9	3.54
	Pull	0.15	2.6	2.88		Pull	0.26	2.9	3.40
	Average	0.17	2.6	3.11		Average	0.28	2.9	3.47
SRC-9	Push	0.33	2.9	3.72	SRC-9	Push	0.33	2.9	3.72
	Pull	0.11	2.4	3.62		Pull	0.11	2.4	3.62
	Average	0.22	2.7	3.67		Average	0.22	2.7	3.67

ratios on shear force is not obvious. Take the Solid - web steel specimens for example, SRC-1 is smaller than SRC-2 by 11%. When it comes to the effects of shaped - steel layouts on ultimate shear, T - shape steel specimens show the best behavior, followed by Solid - web specimens and then the Channel steel specimens. Take the specimens of $T/M = 0.14$ for example, the ultimate shear of SRC-5 is over than SRC-8 by 16%, and the SRC-2 is over than SRC-8 by 11%. Specimens with solid - web steel have the largest ultimate deformation, with the SRC-2 larger than SRC-5 by 20%, and larger than SRC-8 by 16%.

Compared with specimens of $T/M = 0$, the shear bearing capability of specimens under combined torsion does not reduce. As to the displacement, specimens of $T/M = 0$ is larger than that of $T/M = 0.21$, and the displacement will decrease when the T/M ratio increases. So it can be seen that the torque reduce the displacement of specimens.

4.3 Deformation capacity

Ductility factor (μ_{Δ}) is calculated to evaluate ductility of specimens, which is defined as the ratio of ultimate displacement to yield displacement (i.e., $\mu_{\Delta} = \Delta_u/\Delta_y$). Inter - story drift ratio (γ) is calculated to evaluate collapse performance, which is defined as the ratio of displacement to specimen tested length from loading point to the top of base plate (i.e. $\gamma_{cr} = \Delta_{cr}/H$, $\gamma_u = \Delta_u/H$). The measured values of Δ_y and Δ_u are listed in Table 3, and the values of μ and γ are listed in Table 4.

When test finished, the torque does not decrease with the twist angle increases quickly. So we can conclude that when the T/M ratio less than 0.21, the destruction of specimen is dominated by bending. Within the scope of test parameters, the average values of displacement ductility factor for all specimens are between 3.11 and 4.55, larger than Chinese Code for Seismic Design of Building of 3.0.

Displacement ductility of SRC cross - shaped columns is significantly influenced by the T/M ratio: when $T/M = 0.14$ the average ductility is 4.0, when $T/M = 0.21$ the average ductility is 3.5. So as the T/M ratio increases, the displacement ductility decreases. Similarly, the shaped - steel layouts also has important influence on the displacement ductility: the ductility of Solid - web steel specimen is the best by 35% larger than that of T - shaped steel specimen and the Channel steel specimen.

The average displacement ductility of specimens with $T/M = 0$ is 3.7, larger than that of specimens with $T/M = 0.21$. With the increases of T/M ratio, the average displacement ductility will reduce. So it can be seen that the torque reduce the displacement ductility.

The limit of elastic inter - story drift ratio in design code GB50936 - 2014 (2014) is 0.18%, and the elastic - plastic inter - story drift ratio is 2.00% in design code GB50936 - 2014, 0.5% in UBC (1997) and Japan Building Standard Law (2002). It can be seen from Table 4 that the average of crack inter - story drift ratio is 0.21%, the average of ultimate inter - story drift ratio is 2.84%, indicating good deformation abilities of structures under strong earthquakes.

4.4 Energy dissipation

Energy dissipation capacity is regarded as critical

indexes that characterize the seismic performance of structures. In seismic analysis, the energy dissipation capacity is reflected by equivalent damping ratio (h_e), which could be calculated as Eq. (1)

$$h_e = S(ABC + CDA) / (2\pi \cdot S(OBE + ODF)) \quad (1)$$

Where $S_{(ABC+CDA)}$ is the area surrounded by cyclic hysteresis loop and $S_{(OBE+ODF)}$ refers to the sum area of triangle OBE and ODF as shown in Fig. 8. The curve is the first hysteretic loop in each displacement amplitude during displacement - controlled phase. Values of the equivalent damping ratio h_e on various displacement levels $n\Delta_y$ are showed in Table 5 and Fig. 9.

For specimens under combined torsion, torsion energy dissipation capacity increases firstly and then decreases slowly, while bending energy dissipation capacity keeps increasing. When it comes to total energy dissipation capacity, the value keeps stable, although there is a fluctuation in small amplitude.

The total equivalent damping ratio h_e of specimen with $T/M = 0$ is between 0.16 and 0.18, far below the values of specimens with $T/M = 0.14$ and $T/M = 0.21$, which are between 0.24 and 0.29. But the biggest bending equivalent damping ratio of specimens with $T/M = 0$ is larger than that of specimens with torsion. Hence, under the function of torsion, the bending energy dissipation capacity decreases, while the total energy dissipation capacity increases.

The torsion energy dissipation dominates the early loading process until the proportion decreases to 50% of the total energy dissipation at $3\Delta_y$. The proportion of bending energy dissipation increases to 65% when the test finished.

4.5 Stiffness degeneration

Secant stiffness (K) is used to assess stiffness degradation under different lateral displacements and twist angles. Bending stiffness degradation and torsion stiffness degradation are calculated by Eqs. (2) and (3)

$$K_{\Delta} = (|P_j^+| + |P_j^-|) / (|\Delta_j^+| + |\Delta_j^-|) \quad (2)$$

$$K_{\theta} = (|T_j^+| + |T_j^-|) / (|\theta_j^+| + |\theta_j^-|) \quad (3)$$

Where K_{Δ} and K_{θ} are bending stiffness and torsion stiffness corresponding to the peak points of hysteretic,

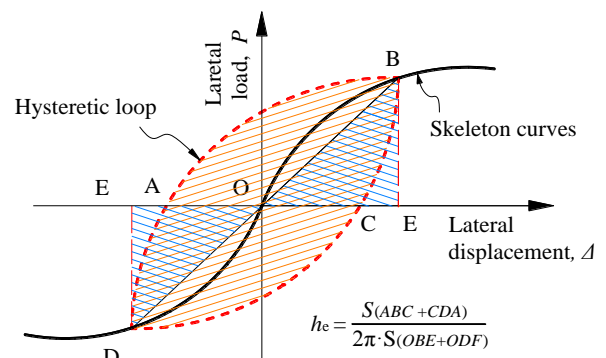


Fig. 8 Calculation diagram of equivalent damping ratio

Table 5 Equivalent damping ratio of specimens

No.	Load	1 Δ_y	2 Δ_y	3 Δ_y	4 Δ_y	5 Δ_y	6 Δ_y	7 Δ_y	8 Δ_y	9 Δ_y
SRC-1	Bending	0.111	0.129	0.114	0.111	0.117	0.123	0.132	0.167	
	Torsion	0.115	0.115	0.097	0.095	0.097	0.097	0.114	0.090	
	Bending +Torsion	0.226	0.244	0.211	0.206	0.214	0.220	0.246	0.257	
SRC-2	Bending	0.115	0.127	0.118	0.122	0.126	0.133	0.142	0.151	0.161
	Torsion	0.147	0.133	0.128	0.113	0.111	0.096	0.101	0.093	0.085
	Bending +Torsion	0.262	0.260	0.246	0.235	0.237	0.229	0.243	0.244	0.246
SRC-3	Bending	0.106	0.144	0.132	0.140	0.166	0.181			
	Torsion	—	—	—	—	—	—	—	—	—
	Bending +Torsion	0.106	0.144	0.132	0.140	0.166	0.181			
SRC-4	Bending	0.103	0.127	0.109	0.106	0.126	0.142	0.151	0.164	
	Torsion	0.100	0.138	0.109	0.100	0.090	0.102	0.091	0.090	
	Bending +Torsion	0.203	0.265	0.218	0.206	0.216	0.244	0.242	0.254	
SRC-5	Bending	0.119	0.116	0.110	0.107	0.122	0.131	0.158	0.173	
	Torsion	0.139	0.157	0.122	0.099	0.093	0.085	0.088	0.087	
	Bending +Torsion	0.284	0.273	0.232	0.206	0.215	0.216	0.246	0.260	
SRC-6	Bending	0.088	0.144	0.156	0.180	0.180				
	Torsion	—	—	—	—	—	—	—	—	—
	Bending +Torsion	0.088	0.144	0.156	0.180	0.180				
SRC-7	Bending	0.105	0.123	0.109	0.119	0.120	0.150	0.174	0.176	
	Torsion	0.101	0.129	0.097	0.100	0.095	0.103	0.083	0.076	
	Bending +Torsion	0.206	0.252	0.206	0.219	0.215	0.253	0.257	0.252	
SRC-8	Bending	0.094	0.124	0.123	0.126	0.136	0.147	0.180	0.199	
	Torsion	0.121	0.168	0.136	0.103	0.086	0.093	0.092	0.087	
	Bending +Torsion	0.215	0.292	0.259	0.229	0.222	0.240	0.272	0.286	
SRC-9	Bending	0.095	0.141	0.167	0.175	0.161				
	Torsion	—	—	—	—	—	—	—	—	—
	Bending +Torsion	0.095	0.141	0.167	0.175	0.161				

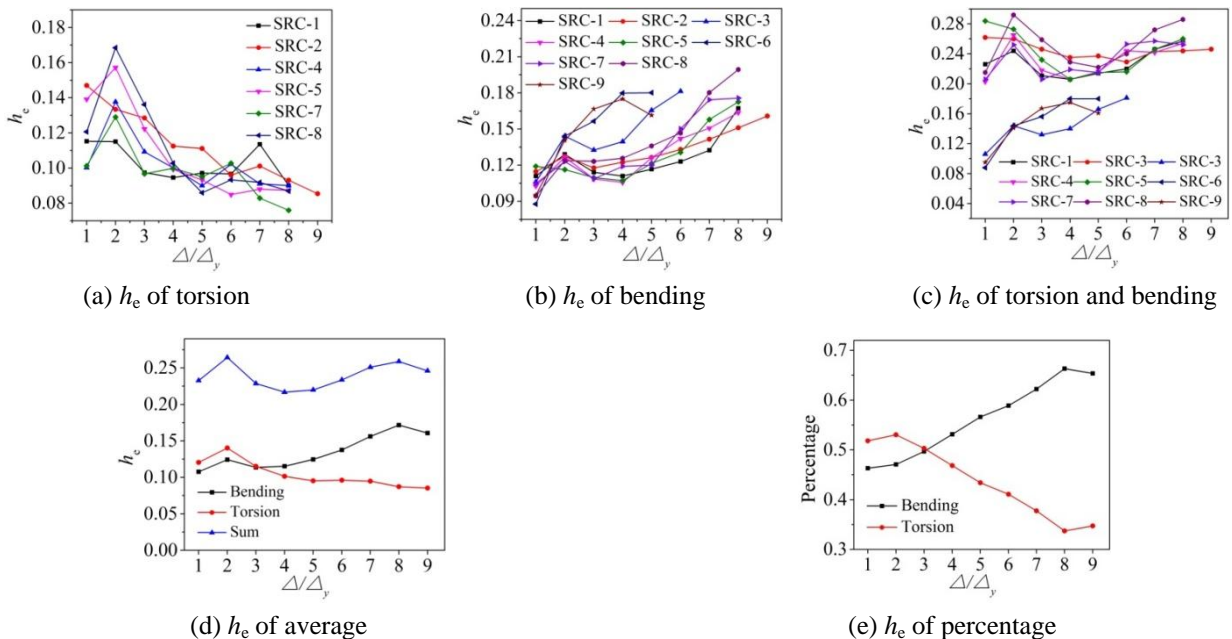


Fig. 9 Equivalent damping ratio curves

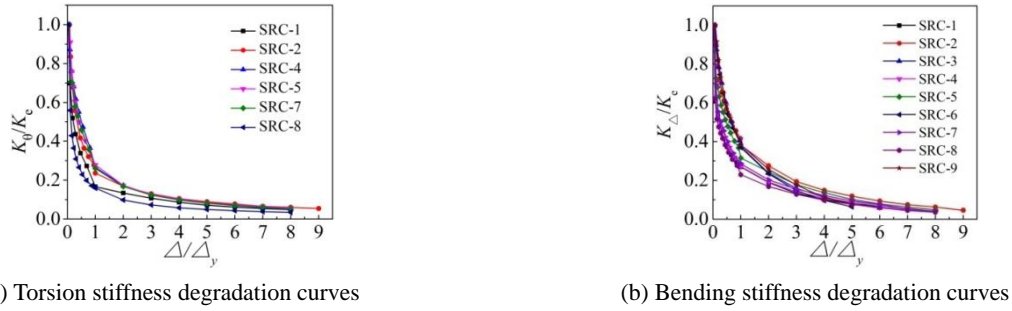


Fig. 10 Stiffness degradation curves

Table 6 Measured torsion secant stiffness at characteristic points

Specimen No.	$K_{\theta y}$ kN·m/(°)	K_c kN·m/(°)	$K_{\theta y}$ kN·m/(°)	$K_{\theta u}$ kN·m/(°)	$K_{\theta cr}/K_{\theta e}$	$K_{\theta y}/K_{\theta e}$	$K_{\theta u}/K_{\theta e}$
SRC-1	542.69	93.85	29.06	13.92	0.17	0.05	0.03
SRC-2	513.67	143.33	30.74	14.00	0.28	0.06	0.03
SRC-4	459.76	114.29	37.26	15.14	0.25	0.08	0.03
SRC-5	531.70	134.44	36.98	17.41	0.25	0.07	0.03
SRC-7	253.52	106.67	33.38	12.33	0.42	0.13	0.05
SRC-8	207.44	118.89	33.10	15.70	0.57	0.16	0.08

Table 7 Measured bending secant stiffness at characteristic points

Specimen No.	$K_{\Delta e}$ kN/mm	$K_{\Delta cr}$ kN/mm	$K_{\Delta y}$ kN/mm	$K_{\Delta p}$ kN/mm	$K_{\Delta u}$ kN/mm	$K_{\Delta cr}/K_{\Delta e}$	$K_{\Delta y}/K_{\Delta e}$	$K_{\Delta p}/K_{\Delta e}$	$K_{\Delta u}/K_{\Delta e}$
SRC-1	74.92	27.22	12.53	5.30	3.27	0.36	0.17	0.07	0.04
SRC-2	51.52	30.59	12.56	5.81	2.95	0.59	0.24	0.11	0.06
SRC-3	42.61	25.38	12.68	6.95	3.19	0.60	0.30	0.16	0.07
SRC-4	74.88	25.60	12.58	6.95	3.59	0.34	0.17	0.09	0.05
SRC-5	59.48	25.17	12.93	7.86	3.75	0.42	0.22	0.13	0.06
SRC-6	40.88	24.44	12.10	8.16	3.85	0.60	0.30	0.20	0.09
SRC-7	66.41	26.00	11.30	6.89	3.72	0.39	0.17	0.10	0.06
SRC-8	70.85	19.70	10.52	5.89	3.13	0.28	0.15	0.08	0.04
SRC-9	38.37	21.54	11.95	6.80	3.30	0.56	0.31	0.18	0.09

respectively; P_j and T_j are peak shear and peak torque under the first cycle of $j\Delta_y$ ($j = 1, 2, 3, \dots$) lateral displacement, respectively; Δ_j and θ_j are displacements and twist angles corresponding to the peak shear and peak torque, respectively; + and - are positive and reverse loading direction, respectively. The stiffness degradation curves are normalized in Fig. 10. Tables 6 and 7 present the secant stiffness at characteristic points, including elastic stiffness (K_e), crack stiffness (K_{cr}), yield stiffness (K_y), peak stiffness (K_p) and ultimate stiffness (K_u).

Compared with bending stiffness, torsion stiffness degradation is faster in the early stage. Both of them have a slowly degradation at the late stage. Tables 6 and 7 show that $K_{\theta y} = 0.05 \sim 0.16 K_{\theta e}$, $K_{\theta m} = 0.03 \sim 0.08 K_{\theta e}$, $K_{\Delta y} = 0.17 \sim 0.31 K_{\Delta e}$, $K_{\Delta u} = 0.07 \sim 0.20 K_{\Delta e}$, $K_{\Delta m} = 0.04 \sim 0.09 K_{\Delta e}$.

Torsion stiffness of specimens with smaller T/M is larger. But in the later stage, torsion stiffness degradation rates of almost all specimens are equal. With the same T/M ratio, elastic stiffness of Channel steel specimens are

smaller than others.

Initial bending stiffness of specimens subjected to pure bending is significant smaller than that subjected to combine torsion. But the stiffness degradation of pure bending specimens is slower in the early stage, which leads to the same bending stiffness as specimens under combine torsion at the later loading process. This illustrates that the addition of torsion can effectively improve the bending elastic stiffness.

4.6 Strength degeneration

Strength degeneration (λ) indicates the strength decrease in different cycles under same lateral displacement. Bending strength degradation and torsion strength degradation are calculated by Eqs. (4) and (5)

$$\lambda_{P_i} = P_j^i / P_j^1 \quad (4)$$

$$\lambda_{T_i} = T_j^i / T_j^1 \quad (5)$$

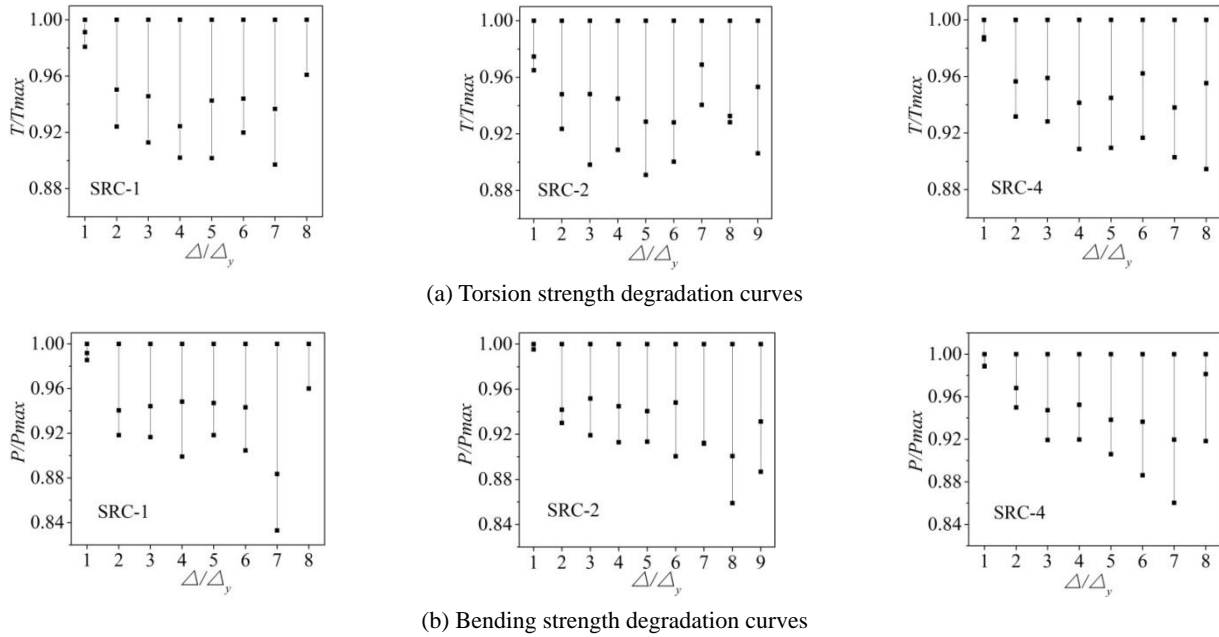


Fig. 11 Strength degradation curves

Where λ_{pj} and λ_{Tj} are bending and torsion strength degeneration, respectively; P_j^i and T_j^i are bending strength and torsion strength under the $j\Delta_y$ ($j = 1, 2, 3\dots$) displacement and twist angle for the i th ($i = 2, 3\dots$) cycle; P_j^1 and T_j^1 are bending strength and torsion strength under $j\Delta_y$ ($j = 1, 2, 3\dots$) displacement and twist angle for the 1st cycle. The changes of specimens strength are plotted in Fig. 11.

Fig. 11 shows that, under the same displacement and twist angle, the bending and torsion strength decrease with the increase of cycles. Comparing the strength degeneration levels of torsion and bending, the former is smaller than the later, with ratios distribute from 0.88 to 0.98 and 0.84 to 0.98, respectively. Under the same displacement, decline proportion of the second cycle is the largest.

4.7 Design suggestion

When structure is designed, torque should be avoid or reduce. It is better to choose Solid-web specimens if the torque is big, while when the bending is big, it is better to chose T-shaped steel specimens. For Solid-web specimens, the bending bearing capacity can be enhanced by improving thickness of flange; the entirety can be increased by adding polypropylene fiber and steel fiber. As to T-shaped steel specimens and Channel steel specimens, enhancing thickness or reducing space of lacing bars can improve the torsion bearing capacity. For Channel steel specimens, the enough thick channel steel is needed.

5. Conclusions

The seismic behavior of SRC cross - shaped columns subjected to combined constant axial load and cyclic flexure - shear - torsion loading is experimentally investigated. The effects of torsion - bending (T/M) ratio and shaped - steel layout are studied by testing nine specimens. These

experimental results and comparisons are indicated as follows:

- In the process of T/M increasing from 0 to 0.21, failure models of SRC cross - shaped columns are bending failure, flexure - torsion failure and torsion - shear failure. The torque - twist angle and shear - displacement hysteretic curves present symmetrical pinched “S” shape, and the latter is plumper than the former.
- Compared with specimens of T/M = 0, the torque less than 0.21 does not reduce the shear capability. It reduces the displacement, displacement ductility and bending energy dissipation capacity, while it increases the total energy dissipation capacity and bending elastic stiffness. When the T/M ratio increases from 0.14 to 0.21, the torque and twist angle increase, but the displacement and displacement ductility decrease.
- With the same T/M ratio, Solid - web steel specimen has the largest torque force, T - shaped steel specimen has the largest shear force, while Channel steel specimen has the smallest torque force and shear force.
- Displacement ductility factor, elastic drift ratio and elastic-plastic drift ratio of SRC cross - shaped columns under combine torsion are over 3.0, 0.0018 and 0.02, respectively, meeting the requirements of China code, American code and Japan code.

In the range of test parameters, the total equivalent damping ratios fall into the range of 0.16 ~ 0.29. The energy dissipation in early period is mainly undertook by torsion while the latter is by flexure. The bending energy dissipation capacity increases with the rising of displacement level, while the torsion energy dissipation capacity decreases.

Acknowledgments

The research reported in this paper was supported by the National Natural Science Foundation of China (N0.51268004 and 51578163), and key project Natural Science Foundation of Guangxi (No: 2016GXNSFDA380032). The writers also appreciate the assistance that was provided by Yuliang Chen, Dingyi Xu, Deyi Xu and Yang Yang during the experimental process.

References

- Anumolu, S., Abdelkarim, O.I. and Elgawady, M.A. (2016), "Behavior of hollow-core steel-concrete-steel columns subjected to torsion loading", *J. Bridge Eng. ASCE* 2016, **21**(10), 04016070.
- Arnold, C. (1980), "Building configuration: Characteristics for seismic design", *Proceedings of the 7th World Conference on Earthquake Engineering*, Istanbul, Turkey, September, **4**, 589-592.
- Belarbi, A., Ayoub, A. and Greene, G. (2007), "Seismic performance of reinforced concrete bridge columns subjected to combined loading including torsion", *Proceedings of Structural Engineering Research Frontiers*, Long Beach, CA, USA, May, pp. 1-16.
- Chen, Z.P., Xu, J.J. and Chen, Y.L. (2016), "Axial compression ratio limit values for steel reinforced concrete (SRC) special shaped columns", *Steel Compos. Struct., Int. J.*, **20**(2), 295-316.
- Deng, J.D., Ma, Z.J. and Liu, A. (2017), "Seismic performance of reinforced concrete bridge columns subjected to combined stresses of compression, bending, shear, and torsion", *J. of Bridge Eng. ASCE* 2017, **22**(11), 04016070.
- Duan, X.N. and Chandler, A.M. (2010), "Seismic torsional response and design procedures for a class of setback frame buildings", *Earthq. Eng. Struct. Dyn.*, **24**(5), 761-777.
- Fang, L., Zhang, B. and Jin, G.F. (2015), "Seismic behavior of concrete-encased steel cross-shaped columns", *J. Construct. Steel Res.*, **109**, 24-33.
- GB/T 50081-2002 (2002), Standard for test method of mechanical properties on ordinary concrete; China Building Industry Press, Beijing, China. [In Chinese]
- GB/T228.1 (2010), Metallic Materials-Tensile Testing – Part 1 Method of Test at Room Temperature; China Standards Press, Beijing, China. [In Chinese]
- GB50936 (2014), Technical code for concrete filled steel tubular structures; China Building Industry Press, Beijing, China. [In Chinese]
- Hsu, H.L. and Wang, C. (2000), "Flexural-torsional behaviour of steel reinforced concrete members subjected to repeated loading", *Earthq. Eng. Struct. Dyn.*, **29**(5), 667-682.
- Hsu, H.L., Hsieh, J.C. and Juang, J. (2004), "Seismic performance of steel-encased composite members with strengthening cross-inclined bars", *J. Construct. Steel Res.*, **60**(3), 1663-1679.
- Japan Building Standard Law (2002), Japan architecture center, Tokyo, Japan. [In Japanese]
- Koliopoulos, P.K. and Chandler, A.M. (1995), "Stochastic linearization of inelastic seismic torsional response: Formulation and case studies", *Eng. Struct.*, **17**(7), 494-504.
- Li, B. and Pham, T.P. (2014), "Experimental study on the seismic response of L-shaped reinforced concrete columns", *Proceedings of Structures Congress 2013: Bridging Your Passion with Your Profession*, Pittsburgh, PA, USA, May, pp. 1673-1682.
- Li, Q. and Belarbi, A. (2012), "Performance based design approach for RC square bridge columns under combined loadings including torsion", *Proceedings of Structure Congress 2012*, Chicago, IL, USA, March, pp. 2223-2234.
- Li, Q. and Belarbi, A. (2013), "Damage assessment of square RC bridge columns subjected to torsion combined with axial compression, flexure, and shear", *KSCE J. Civil Eng.*, **17**(3), 530-539.
- Liang, Q.Q., Uy, B. and Liew, J.Y.R. (2008), "Local buckling of steel plates in concrete-filled thin-walled steel tubular beam-columns", *Steel Construct.*, **63**(3), 396-405.
- Liu, Z.Q., Xue, J.Y. and Zhao, H.T. (2016), "Seismic behavior of steel reinforced concrete special-shaped column-beam joints", *Earthq. Struct.*, **11**(4), 665-680.
- Liu, Z.Q., Xue, J.Y. and Zhao, H.T. (2016), "Seismic behavior of steel reinforced concrete special-shaped column-beam joints", *Earthq. Struct.*, **11**(4), 665-680.
- Mullapudi, T.R.S. (2013), "Seismic analysis of reinforced concrete structures subjected to combined axial, flexure, shear and torsional loads", *J. Struct. Eng. ASCE* 2013, **139**(4), 561-573.
- Nie, J.G., Wang, Y.H. and Fan, J.S. (2012), "Experimental study on seismic behavior of concrete filled steel tube columns under pure torsion and compression-torsion cyclic load", *J. Construct. Steel Res.*, **79**(1), 115-126.
- Nie, J.G., Wang, Y.H. and Fan, J.S. (2013), "Experimental research on concrete filled steel tube columns under combined compression-bending-torsion cyclic load", *Thin-Wall. Struct.*, **67**(2), 1-14.
- Otsuka, H., Takeshita, E. and Urakawa, Y. (2005), "Seismic performance and correlation characteristics of reinforced concrete columns subjected to torsional moment, bending moment/shear force and axial force", *Proceedings-Japan Society of Civil Engineers*, Volume 801, pp. 123-139.
- Patton, M.L. and Singh, K.D. (2012), "Numerical modeling of lean duplex stainless steel hollow columns of square, L-, T-, and + -shaped cross sections under pure axial compression", *Thin-Wall. Struct.*, **53**, 1-8.
- Patton, M.L. and Singh, K.D. (2014), "Finite element modelling of concrete-filled lean duplex stainless steel tubular stub columns", *Int. J. Steel Struct.*, **14**(3), 619-632.
- Prakash, S., Belarbi, A. and You, Y.M. (2010), "Seismic performance of circular RC columns subjected to axial force, bending, and torsion with low and moderate shear", *Steel Construct.*, **32**(1), 46-59.
- Ramamurthy, L.N. and Khan, T.A.H. (1986), "Closure of L-Shaped Column Design for Biaxial Eccentricity", *J. Struct. Eng.*, **112**(10), 2360-2362.
- Sun, R., Burgess, I.W. and Huang, Z. (2015), "Progressive failure modelling and ductility demand of steel beam-to-column connections in fire", *Eng. Struct.*, **89**(17), 66-78.
- Tirasit, P. and Kawashima, K. (2007), "Seismic performance of square reinforced concrete columns under combined cyclic flexural and torsional loadings", *J. Earthq. Eng.*, **11**(3), 425-452.
- UBC (1997), Uniform Building Code; International Council of Building Officials (ICBO), CA, USA.
- Wang, P., Han, Q. and Du, X.L. (2014), "Seismic performance of circular RC bridge columns with flexure-torsion interaction", *Soil Dyn. Earthq. Eng.*, **66**, 13-30.
- Xiang, P., Deng, Z.H. and Su, Y.S. (2017), "Experimental investigation on joints between steel-reinforced concrete T-shaped column and reinforced concrete beam under bidirectional low-cyclic reversed loading", *Adv. Struct. Eng.*, **20**(3), 446-460.
- Yang, Y., Yang, H. and Zhang, S. (2010), "Compressive behavior of T-shaped concrete filled steel tubular columns", *Int. J. Steel Struct.*, **10**(4), 419-430.
- Zhou, T., Chen, Z. and Liu, H. (2012), "Seismic behavior of special shaped column composed of concrete filled steel tubes", *J. Construct. Steel Res.*, **75**, 131-141.

Zuo, Z.L., Cai, J. and Yang, C. (2012), "Axial load behavior of L-shaped CFT stub columns with binding bars", *Eng. Struct.*, **37**, 88-98.

CC